J Mater Sci (2010) 45:2203–2209
DOI 10.1007/s10853-009-4060-0

HTC2009

Influence of processing route on electrical and thermal conductivity of Al/SiC composites with bimodal particle distribution

L. Weber · G. Sinicco · J. M. Molina

Received: 2 June 2009 / Accepted: 21 November 2009 / Published online: 10 December 2009

Abstract Al/SiC composites with volume fractions of SiC between 0.55 and 0.71 were made from identical tapped and vibrated powder preforms by squeeze casting (SC) and by two different setups for gas pressure infiltration (GPI), one that allows short (1–2 min) liquid metal/ceramic contact time (fast GPI) and the other that operates with rather long contact time, i.e., 10–15 min, (slow GPI). Increased liquid metal–ceramic contact time is shown to be the key parameter for the resulting thermal and electrical conductivity in the Al/SiC composites for a given preform. While for the squeeze cast samples neither dissolution of the SiC nor formation of Al_4C_3 was observed, the gas pressure assisted infiltration led inevitably to a reduced electrical and thermal conductivity of the matrix due to partial decomposition of SiC leading to Si in the matrix. Concomitantly, formation of Al_4C_3 at the interface was observed in both sets of gas pressure infiltrated samples. Longer contact times lead to much higher levels of Si in the matrix and to more Al_4C_3 formation at the interface. The difference in thermal conductivity between the SC samples and the fast GPI samples could be rationalized by the reduced matrix thermal conductivity only. On the other hand, in order to rationalize the thermal conductivity of the slow GPI a reduction in the metal/ceramic interface thermal conductance due to excessive Al_4C_3-formation had to be invoked. The CTE of the composites generally tended to decrease with increasing volume fraction of SiC except for the samples in which a large expansive drift was observed during the CTE measurement by thermal cycles. Such drift was essentially observed in the SC samples with high volume fraction of SiC while it was much smaller for the GPI samples.

Introduction

Al/SiC composites have been a research subject for over 20 years [1–4] and are now becoming a commodity in thermal management applications [5–7]. Industrial grades of Al–SiC have thermal conductivity in the range from 170 to 200 W/mK [5, 8]. Such relatively low values are on the one hand due to the use of Si- and Mg-containing matrices (to prevent Al_4C_3 formation and for pressureless infiltration [6, 9–13]) on the other hand residues of binders used for fabrication of self-standing preforms may further reduce thermal conductivity of the composites [8]. Third, in order to reach the required low level of CTE, high volume fractions of SiC are necessary that can only be achieved by using SiC with a bi- or trimodal size distribution [6, 14, 15]. This leads to a reduced effective thermal conductivity of the small particles due to larger contributions of the interface thermal resistance between matrix and composite.

In the present contribution, we investigate the potential of using pure aluminum as a matrix with the aim to improve the thermal conductivity of the composite. Since SiC is not stable in liquid aluminum [16] we vary the liquid metal/ceramic contact time to investigate the effect of reaction on the physical properties of the resulting

G. Sinicco—formerly an undergraduate student of École Polytechnique Fédérale de Lausanne, EPFL.

L. Weber (✉) · G. Sinicco · J. M. Molina
Laboratory of Mechanical Metallurgy, École Polytechnique Fédérale de Lausanne, EPFL, 1015 Lausanne, Switzerland
e-mail: ludger.weber@epfl.ch

Present Address:
J. M. Molina
Instituto Universitario de Materiales de Alicante, Universidad de Alicante, Apto 99, 03080 Alicante, Spain

composites. Results are put in perspective with expectations based on currently accepted modeling schemes.

Experimental procedures

Powder mixtures of green α-SiC HD (from SaintGobain, Norway) of powders with grit size F100 and F500 corresponding to a nominal average particle diameter of 167 and 16 μm, respectively, where prepared by dry mixing of powders. Six mixtures with volume fraction of large (F100) particles of 20, 30, 40, 50, 60, and 70% were prepared and their packing density was determined after tapping and vibrating them into a graded recipient of similar diameter as the infiltration molds.

The infiltration mold was a graphite cylinder with seven slightly conical holes with length 36 mm and mean diameter of roughly 12.8 mm, cf. Fig. 1. At the lower end of the conical part, a continuation in a cylindrical hole with reduced diameter (4 mm) was added to facilitate demolding after infiltration while maintaining a well defined sample geometry. Furthermore, these small diameter cylindrical prolongations were used for CTE measurement of the composites. A series of small holes was machined at 4 mm from the bottom and the top of the conical part of the mold to place graphite mines of 0.9 mm diameter to diagonally cross the cavities. The purpose of these rods was to facilitate the drilling of holes for the thermocouples needed for the thermal conductivity measurement.

The powder mixtures were filled in the holes by tapping and vibrating. The seventh cavity was filled with the "pure" F500 powder. Three such molds were prepared, one for squeeze casting the other two for gas pressure assisted infiltration. The mold for squeeze casting was mounted in a steel rig that could be attached at the bottom of the squeeze-casting cavity. For squeeze casting the mold containing the seven preforms was pre-heated to 550 °C and the liquid aluminum (99.99% from Norsk Hydro, Grevenbroich, Germany) was preheated to 750 °C. The casting cavity and the ram were preheated to 300 °C and coated with graphite spray. Once the liquid metal was purred in the casting cavity the ram was lowered at 10 mm/s up to a maximum pressure of 100 MPa. Solidification took place in less than 30 s.

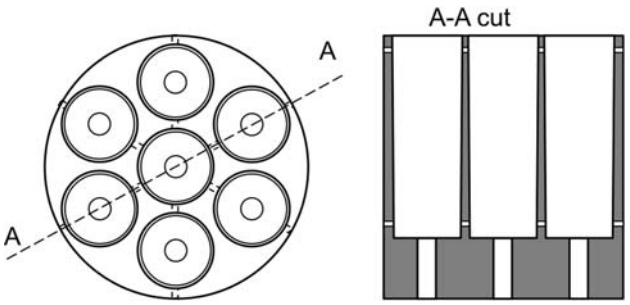

Fig. 1 Sketch of the 7-hole-mold used for the simultaneous infiltration of the series of SiC preforms

The mold for slow gas pressure infiltration (GPI) was placed in an alumina crucible and held in place by a graphite disc containing seven holes allowing the metal to easily enter into the preform. Pure aluminum pieces from the same batch as for squeeze casting were placed on top of the graphite plate. The alumina crucible with the graphite mold containing the preforms and the aluminum was put in a custom-made cold-wall GPI apparatus. A vacuum of 3 Pa was pulled slowly in the infiltration chamber. Once vacuum was reached, the batch was heated by an induction coil/graphite susceptor couple. The heating rate was roughly 200 K/h. After reaching a temperature of 750 °C the system was allowed to stabilize for 30 min while still pulling the vacuum. Argon gas pressure of 5 MPa was applied at 1 MPa/min and the heating was switched off once the pressure was reached. Cool-down of the casting was measured with two thermocouples, one between susceptor and alumina crucible and one just above the liquid metal. The cooling rate was of the order of 10–15 K/min leading to a liquid metal/reinforcement contact time of at least 10 min.

For the fast GPI the mold was inserted in a hBN-coated steel crucible. The space of about 1 mm width between mold and crucible was filled with very fine (<1 μm) alumina powder. This prevented the metal to go around the mold during infiltration and thus held the mold in place. A layer of Safimax alumina wool was placed between the metal ingot and the SiC-filled mold to prevent premature contact of liquid metal and the preform before pressurization. The steel crucible was inserted in a AISI 316L container with threaded caps on either side and sealed with a 0.2 mm Graphoil (GrafTech Int'l, Lakewood, OH) seal. A gas and vacuum line was welded to the upper cap. Vacuum was pulled slowly and once a pressure below 50 Pa was reached, the container was inserted in a vertical furnace preheated to 300 °C while still pumping the vacuum. After 1 h, the furnace temperature was increased to 750 °C and the set-up was left in the furnace for 3 h to reach equilibrium. The container was taken out of the furnace and its bottom cap was quenched in water while pressure of 5 MPa was rapidly applied, i.e., within a few seconds. After 1 min the whole container was dumped in the water.

The samples of both GPI castings were pushed out of the graphite mold whereas the SC sample had to be machined out of the mold. Composite characterization comprised microstructural analysis by standard optical metallography, density measurements to derive effective volume fraction of SiC in the composites, and measurement of thermal and electrical conductivity. Electrical conductivity was measured using an Eddy-current-based Sigmatest 2.069 (Foerster, Pittsburgh, PA) on the flat faces of the thermal conductivity samples.

The thermal conductivity was measured in a custom-made comparative steady state rig against a copper and a brass reference. The set-up was calibrated against a sample of pure aluminum ($k = 237$ W/mK) to yield conductivities of the Cu and the brass of 398 and 108 W/mK, respectively. The slightly conical samples were clamped between the reference heated by a thermally stabilized water bath and a water-cooled support. Under the assumption of no radial heat loss, the heat flux through sample and reference are equal and the thermal conductivity of the sample can be determined based on the ratio of the temperature gradients in the sample and the reference and the thermal conductivity of the reference. Since drilling of the holes to place the thermocouples would have been nearly impossible in the Al/SiC, the graphite mines had been set already in the preform and were easy to remove after infiltration. The conductivities were measured slightly above room temperature in the as-cast condition, after a heat treatment of 1 h at 550 °C, and after a heat treatment at 550 °C including furnace cool-down to 350 °C and subsequent hold for 40 h at this temperature.

CTE measurements were conducted in a Netzsch TMA 402 (Netzsch, Selb, Germany) by two cycles between −50 and 200 °C with a nominal heating and cooling speed of 5 K/min and a hold of 10 min at each temperature extremum.

Results

Optical microscopy of the samples revealed homogeneous distribution of the SiC in the aluminum matrix as well as homogeneous distributions of the large particles with a bed of small particles up to 60 pct of large particle. For 70 pct of large particles the spaces between the touching large particles were somewhat irregularly filled with the small particles, cf. Fig. 2a, b. At high magnification, Fig. 2c, d,

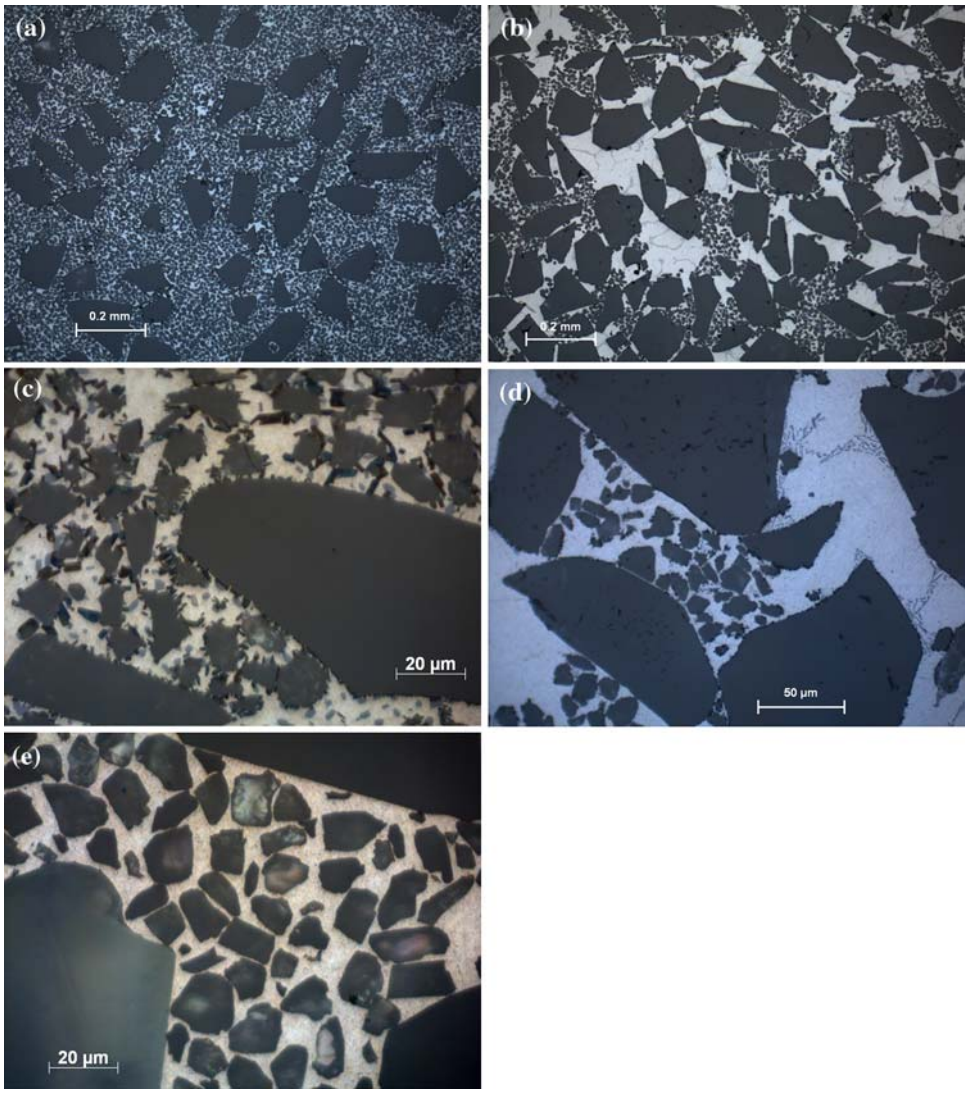

Fig. 2 Optical micrographs of the infiltrated samples showing: **a** homogeneous distribution of the large particles in a bed of small particles (30% of large particles, GPI slow); **b** inhomogeneous filling of the spaces between large particles (70% of large particles, GPI fast); **c** microstructure with large amount of Si and Al_4C_3 (60% of large particles, GPI slow); **d** microstructure with little Si and Al_4C_3 (70% of large particles, GPI fast); **e** microstructure free of Si and Al_4C_3 (60% of large particles, SC)

islands of Si phase and another, darker phase, presumably Al_4C_3, could be observed in the GPI samples while the squeeze cast sample was free of Si-phase and Al_4C_3, cf. Fig. 2e. In the samples with 70 pct of large particles the Si-content in the matrix could be appreciated from looking at the areas were no small particles were present. The Si content in the matrix is visibly much higher in the slow GPI samples than in their rapidly cooled counterparts, cf. Fig. 2c, d. Concomitantly, the amount of the darker phase was less in the rapidly cooled GPI samples than in the slowly cooled samples.

Density measurements of the composites indicated that for the squeeze cast samples and for the fast GPI samples the packing density of SiC in the composite was 2–3 vol pct lower than that determined in the powder packing experiments, Fig. 3. In the composites processed by GPI, this difference was even somewhat larger at high volume fractions of large particles.

Electrical conductivity of the composite samples is shown in Fig. 4 as a function of the total SiC volume fraction. The indicated values are averages of the conductivity measured on the two faces of the thermal conductivity samples after the heat treatment, except for the slow GPI sample with 60 pct of large particles that showed a significantly larger amount of shrinkage porosity on the upper face of the sample. The SC samples have for a given volume fraction of SiC a significantly higher electrical conductivity, while the fast GPI samples are only slightly more conducting than their slow GPI counterparts. Compared to the as cast condition the electrical conductivity of the fast GPI samples increased by a little less than 10% on average.

The thermal conductivities of the various samples are given in Fig. 5. For the squeeze cast samples, thermal conductivity was unaffected by the various heat treatments and stayed for all powder mixtures between 225 and

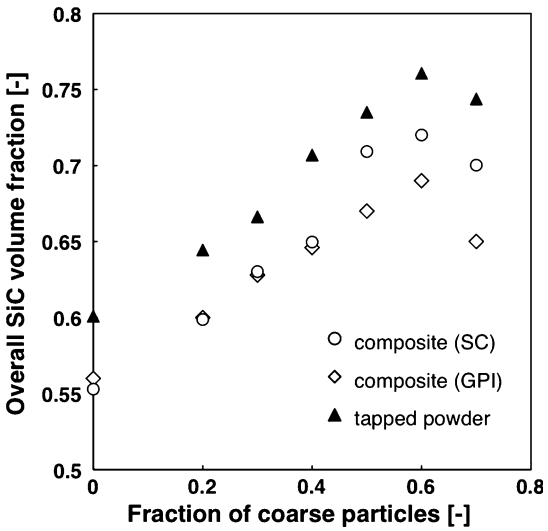

Fig. 3 Evolution of the overall volume fraction of SiC in the packed powder beds and the composites as derived from density measurement as a function of the mixing ratio of large (F100) and small (F500) SiC particles

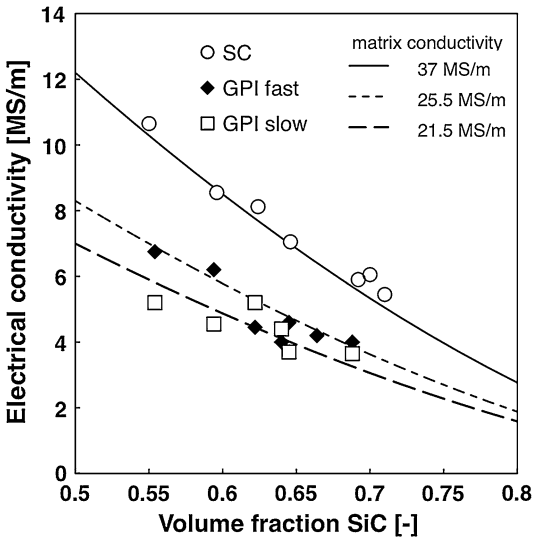

Fig. 4 Evolution of the electrical conductivity with the total SiC volume fraction for the three series of composites. The predicted values according to the DEM are also included in the graph. The deduced matrix conductivity is 37, 25.5, and 21.5 MS/m for the SC, GPI fast, and GPI slow series, respectively

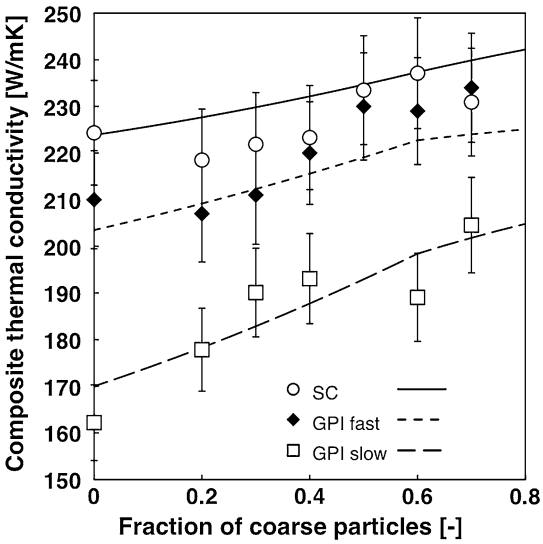

Fig. 5 Thermal conductivity of the SiC/Al composites produced through infiltration of aluminum into preforms of mono- and bimodal SiC mixtures (SiC-500/SiC-100) versus the percentage of coarse particles. The lines correspond to the calculation with using the values of, and h given in Table 1

235 W/mK with a slight tendency to increase with the amount of large particles. For the samples prepared by fast GPI, the thermal conductivity increased from around 200 W/mK for the composite containing only small particles with increasing fraction of large particles up to 230 W/mK. For the slow GPI samples, values increased from 160 to 205 W/mK with increasing fraction of large particles. Values measured after the solutionizing treatment at 560 °C were on average somewhat lower than in the as cast and the precipitation treated samples.

The results of the CTE measurements are collected in Fig. 6. The physical CTEs (measured in a range of ±5 K around the indicated temperature) are given for the SC and the fast GPI samples only, yet for two temperatures of technical interest, i.e., ambient temperature (298 K) and 398 K. The CTE decreases in general with increasing SiC volume fraction and is typically 1–1.5 ppm/K higher at 398 K than at ambient temperature. For the SC samples with high volume fractions some residual increase in length was observed during the two temperature cycles of the measurements the amplitude of which is indicated as average drift on the right hand *y*-axis in Fig. 6. Therefore, these samples have an apparent higher CTE than expected from their volume fraction of SiC. For the GPI samples the drift was much smaller for all samples.

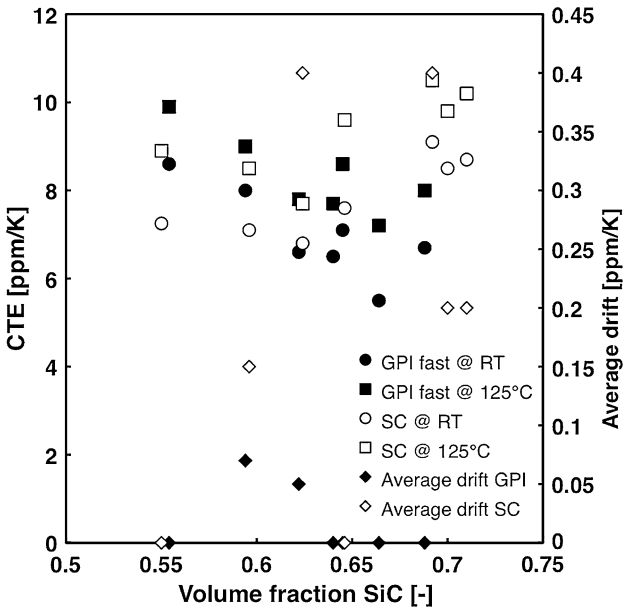

Fig. 6 Physical CTEs of the composites made by fast GPI and SC for temperatures of 298 and 398 K. The CTE decreases in general with increasing volume fraction of SiC. The CTE is typically 1–1.5 ppm/K higher at 398 K compared to the values at 298 K. For the SC samples with highest volume fraction a residual elongation after the two temperature cycles was visible being indicated as the average drift on the right hand *y*-axis. For the GPI samples the drift was systematically much lower or even absent

Discussion

The optical micrographs in Fig. 2 give clear evidence for the expected tendency that the propensity of SiC dissolution and formation of an additional phase from the interface increases with increasing liquid metal/ceramic contact time. Although we have no analytical evidence that the darker phase is in fact Al_4C_3, the morphology and thermodynamic considerations support this conjecture.

Densitometry indicates a systematic difference between the volume fraction obtained in the composite and that expected from packing experiments. There are at least two phenomena that could be invoked to rationalize this: (i) the packing and vibrating in a dedicated graded quartz vial is more efficient than in a graphite mold; and (ii) due to the quite small difference in density between SiC and the metal, the presence of minute quantities of porosity due to differential thermal contraction of the constituents upon cooling after solidification or during solidification itself may lower the apparent particle volume fraction quite significantly. The shrinkage porosity, V_p, due to differential thermal expansion can be estimated as

$$V_p \approx (T - T_m)(\alpha_{Al} - \alpha_{SiC})V_m \quad (1)$$

where T and T_m denote the temperature of consideration and the solidification temperature of the matrix, respectively, α designates the coefficient of thermal expansion with the index indicating the respective phase, and V_m is the matrix volume fraction. The shrinkage porosity is thus estimated to be in the order of 0.5 vol pct, in reasonable agreement with tomography measurements on a comparable Al/diamond composite [17]. Such a level of shrinkage porosity would lead to an underestimation of the particle volume fraction in the order of 3 vol pct.

A further difficulty appears when additional phases are involved. If SiC is partially dissolved the average density of the matrix (including now some Si) and the particles (lined with a carbon or carbide layer) is lowered which may serve as a rational why the GPI samples seem to have somewhat lower volume fractions than their SC counterparts. In view of the many intervening parameters (volume fraction and density of all reaction products) a precise quantitative analysis of this effect is beyond the scope of the present contribution. With the caveats in mind, we indicate as the volume fraction of the composites the one deduced from densitometry under the assumption that only two phases are present, which represents a lower limit for the effective volume fraction.

The electrical conductivity as a function of the volume fraction of non-conducting particles can be analyzed in terms of the differential effective medium (DEM) scheme that has been shown to be appropriate for modeling conductivity of composites at high volume fraction and high

phase contrast [18]. For the case of non-conducting inclusions in a conducting matrix the DEM scheme takes the following simple form:

$$\sigma_c = \sigma_m V_m^n \quad (2)$$

where σ_c and σ_m stand for the composite and the matrix conductivity, V_m denotes the matrix volume fraction and n is a parameter accounting for the particle shape being typically in the range between 1.5 (for spheres) and 1.8 (for oblate spheroids with an aspect ratio of roughly 5). The fits included in Fig. 4 indicate a shape factor of 1.62 and a matrix electrical conductivity of 37.5, 25.5, and 21.5 MS/m for the SC, fast GPI, and slow GPI samples, respectively. The electrical conductivity of pure Al is typically at 37.3 MS/m [19]. Therefore, the electrical conductivity measurements give evidence that indeed the dissolution of SiC in the squeeze casting process is negligible. On the other hand, the difference between the two GPI processes is rather small being mainly due to the difference in volume fraction of Si particles in the matrix as evidenced in Fig. 2c, d while the level of residual Si in solid solution is the main reason for reduced electrical conductivity as compared to the SC samples.

The thermal conductivity of the two series was modeled according to a recently proposed generalized differential effective medium scheme capable of taking into account more than one type of inclusions [14]. The reason to treat the SiC inclusions of different sizes as two distinct inclusion phases resides in the fact that due to their difference in size their effective thermal conductivity (i.e., the conductivity taking into account the influence of a finite interface thermal conductance) is different. The effective conductivity, κ_p^{eff}, of a (spherical) inclusion is linked [14] to its intrinsic conductivity, κ_p^{int}, the interface thermal conductance, h, and the particle radius, r, by

$$\kappa_p^{eff} = \frac{\kappa_p^{int}}{1 + \frac{\kappa_p^{int}}{rh}} \quad (3)$$

The free parameters for the modeling are the thermal conductivity of the matrix and the inclusion as well as the interface thermal conductance, h. The values adopted for these parameters to fit the three sets of data are given in Table 1. For consistency, the intrinsic conductivity of the SiC has to be the same for all three series. We find that a value of 255 W/mK fits our data best. This is in general agreement with other investigations [14] although the green SiC for that study had been from a different source. Furthermore, the matrix conductivity in the squeeze cast samples is that of pure aluminum due to the lack of time to react with the reinforcement. In the case of the gas pressure infiltrated samples, the matrix had time to react with the SiC, as evidenced by the micrographs, Fig. 2c, d, and its conductivity is that of an Al–Si alloy. In a previous contribution, we have determined the thermal conductivity of an Al–Si matrix as present after infiltration of pure Al into SiC to be around 185 W/mK [14] for which intermediate reaction times were used. We therefore have chosen 170 W/mK for the matrix after slow GPI and 190 W/mK after fast GPI. Most interestingly, the interface thermal conductance required to fit the evolution of the composite conductivity is different for the squeeze cast samples and the fast GPI as compared to the slow GPI samples. For the former we find an interface thermal conductance of $1.4\ 10^8$ W/m^{2}K which is slightly higher than that found in earlier work in the same system [14]. However, in the slow GPI samples, h is reduced to roughly half this value, most likely due to the abundant Al_4C_3 reaction at the interface. We note in passing that the h value found in our previous study was intermediate to the two values found in this study, as were the liquid metal contact times and the thermal conductivity of the composite.

Table 1 Modelling parameters used for the three different series of infiltrated samples

Data set	κ_m (W/mK)	κ_{SiC} (W/mK)	h (W/m^{2}K)
SC	236	255	1.4×10^8
GPI fast	190	255	1.4×10^8
GPI slow	170	255	7×10^7

Conclusion

We conclude that the use of pure aluminum for liquid metal infiltration into SiC leads only for the case of short to very short contact times to an improvement of thermal and electrical conductivity as compared to the industrial grade composites with high Si contents in the matrix. Even at relatively short liquid solid contact times, in the order of 1 min, the electrical conductivity is significantly reduced due to dissolution of Si in the matrix. Subsequent heat treatment cannot restore the high electrical conductivity of the pure Al matrix composites obtained after squeeze casting. At contact times longer than several minutes the interface reaction between melt and SiC particles leads to significant reduction in thermal conductivity. Additionally, the material gets prone to degradation at ambient conditions due to swelling during the reaction of Al_4C_3 with humidity.

Acknowledgements One of the authors (G. S.) acknowledges funding by the EU FP6 integrated project "ExtreMat" under the contract no. NMPCT-2004-500253. Disclaimer: The work reflects only the views of the authors and the EU in not liable for any use of the information contained therein. J. M. Molina also acknowledges funds from the Generalitat Valenciana (project GVPRE/2008/244)

and Universidad de Alicante (project GRE08-P13). J. M. Molina is also grateful to the Spanish Ministerio de Educación y Cultura for his "Juan de la Cierva" contract.

References

1. Zweben C (1992) J Met 44:15
2. Zweben C (1998) J Met 50:47
3. Zweben C (2005) Adv Mater Process 163:33
4. Zweben C (2006) Power Electron Technol 32:40
5. Occhionero MA, Fennessy KP, Adams RW, Sundberg GJ (2009) http://www.alsic.com/papers/cps_igbt_2001.pdf, viewed May 14
6. Occhionero MA, Hay RA, Adams RW, Fennessy KP (1998) Proceedings of SPIE—The international society for optical engineering 3582, p 687
7. Occhionero MA, Hay RA, Adams RW, Fennessy KP (1999) In: Wong CP (ed) IMAPS Advanced packaging symposium. Chateau Elan, Braselton, Georgia
8. Lee HS, Jeon KY, Kim HY, Hong SH (2000) J Mater Sci 35:6231. doi:10.1023/A:1026749831726
9. Zhang Q, Wu G, Chen G, Jiang L, Luan B (2003) Compos A 34:1023
10. Lloyd DJ (1994) Int Mater Rev 39:1
11. Pech-Canul MI, Katz RN, Makhlouf MM, Pickard S (2000) J Mater Sci 35:2167. doi:10.1023/A:100475830580
12. Han G, Feng D (2000) J Mater Sci Technol 16:460
13. Zulfia A, Hand R (2000) J Mater Sci Technol 16:867
14. Molina JM, Narciso J, Weber L, Mortensen A, Louis E (2008) Mater Sci Eng A 480:483
15. Zhang Q, Wu G, Jiang L, Luan B (2005) Phys Status Solidi A Appl Res 202:1033
16. Lloyd DJ (1989) Compos Sci Technol 35:159
17. Schöbel M, Fiedler G, Degischer HP, Altendorfer W, Vaucher S (2009) Adv Mater Res 59:177
18. Weber L, Dorn J, Mortensen A (2003) Acta Mater 51:3199
19. Bass J (1982) In: Bass J, Fischer KH (eds) Landolt-Börnstein: numerical data and functional relationships in science and technology new series III/15: metals: electronic transport phenomena. Springer-Verlag, Berlin, p 5